PREPRINT- Final published version may differ in minor details
Materials Research Society Symposium Proceedings **1514**:99-104 2013

Effect of Alloy Composition & Helium ion-irradiation on the Mechanical Properties of Tungsten, Tungsten-Tantalum & Tungsten-Rhenium for Fusion Power Applications

Christian E. Beck[1], David E. J. Armstrong[1], Philip D. Edmondson[1] and Steve G. Roberts[1]
[1]Department of Materials, University of Oxford, Parks Road, Oxford, OX1 3PH, UK

ABSTRACT

Model alloys have been made of pure W and 1% & 5% W-Ta and W-Re. Indentation hardness and modulus data were obtained by nanoindentation to assess the effect of composition on mechanical properties. Results showed that both the Ta and Re compositions hardened with increasing alloy content, greater in the W-5%Ta composition which showed an increase of 1.03GPa (17%), compared to a 0.43GPa (7%) increase in W-5%Re. The samples also showed very small increases in modulus of ~ 25GPa (6%) in both W-5%Re and W-5%Ta. The samples were implanted with 3000appm concentration of helium. All samples show a substantial increase in hardness of up to 107% in the case of pure W. An appreciable difference in modulus is also seen in all samples. Initial TEM work has shown no visible He bubbles, suggesting that the mechanical properties changes are due to He-vacancy cluster formation below the resolvable limit.

INRODUCTION

Tungsten-based alloys are being considered as likely candidate materials for plasma-facing components in a nuclear fusion reactor. Structural components in the divertor and particularly the divertor plate will potentially be exposed to maximum operating temperatures in excess of 1000°C whilst being bombarded with 14.1MeV neutrons producing displacement damage of up to 150dpa over the divertor lifetime [1]. In addition to the cascade damage produced, helium retention in the first wall material from direct injection of plasma ions and neutron-induced transmutation events also has the potential to produce microstructural changes and in turn significant mechanical changes, although these are as yet not well characterised [2-4]. Tungsten-based alloys represent the greatest hope of being able to eventually fulfil the material requirements due to their high melting point (3695K), good resistance to sputtering and void swelling, relatively low tritium retention rates and good thermal resistance and conductivity properties, which remain stable under irradiation [5-6]. Tungsten alloys however have some drawbacks: high ductile to brittle transition temperature (DBTT), susceptibility to radiation embrittlement and processing issues due to their high melting temperature will have to be overcome [2,7-8].

The effect of alloying additions on the properties of tungsten is of interest for two reasons: firstly, deliberate alloying has the potential to improve material properties and secondly, to assess the effects of 'transmutation alloying'. Modelling has shown that over a 5 year service period for divertor conditions in a fusion power plant such as DEMO, over 5% of the tungsten would be transmuted, with rhenium and tantalum being two of the most significant transmutants [9]. It is therefore important that the effects of these alloying additions on the mechanical properties of model systems is understood both pre and post irradiation. There has also been

speculation that tantalum like, rhenium and iridium, could have beneficial effects on the ductility of tungsten [10].

Due to the lack of a suitable facility to produce the level of neutron irradiation and helium implantation that a first-wall material would experience in a fusion power reactor and the inability to simulate reactor lifetime over laboratory time-scales, ion implantation techniques have been used to simulate the cascade and implantation damage [11-12]. Damage produced by ion implantation techniques is shallow – typically on the scale of a few hundred nm to several μm beneath the implanted surface. This necessitates the use of micromechanical testing techniques such as nanoindentation [12,13].

Helium damage is of particular interest as significant microstructural changes have been demonstrated in polycrystalline tungsten under helium implantation, potentially producing large changes in mechanical and thermal properties [2,6,14]. These changes can be substantially greater than those of self-ion implantation (cascade) damage alone [12]. Doses of up to 1500appm could be expected to be observed in first wall reactor materials [1]. Relatively little work has been done to date to characterise the effect of helium implantation on these alloys, either with or without concomitant displacement damage. This paper reports a nanoindentation study of the effects of helium implantation on the mechanical properties of W and dilute W-Re and W-Ta alloys.

EXPERIMENTAL DETAILS

Model alloys of 1 & 5% Re & Ta were produced by the arc-melting of high-purity elemental powders: 99.9% Ta & W, (Sigma Aldrich, USA) 99.99%Re (AEE, USA). The powders were weighed and mixed in a Turbula powder mixer (WAB, Switzerland) and compressed using a uniaxial press. The resultant pellets were melt-processed using a plasma-arc furnace in an argon atmosphere at the Department of Materials Science & Metallurgy at the University of Cambridge. The slugs produced were sliced into sheets and polished using diamond paste followed by a 50nm colloidal silica suspension to produce a high quality damage-free surface finish. Figure 1 shows typical microstructures as electron back-scatter diffraction (EBSD) inverse pole figure (IPF) maps, produced using Orientation Imaging Microscopy (OIM) software (EDAX-TSL, AMETEK, USA). In all materials, grains were equiaxed, of size ~50μm-500μm and without any significant texture.

Mechanical data were obtained from both irradiated and unirradiated samples by nanoindentation using an MTS NanoXP (Agilent, USA), using a Berkovich diamond indenter to a maximum depth of 2μm. The continuous stiffness measurement method (CSM) was used to evaluate the hardness and elastic modulus as a function of indentation depth without the need to run multiple load-unload cycles [15]. Grids of indents were placed over several grains for each alloy type.

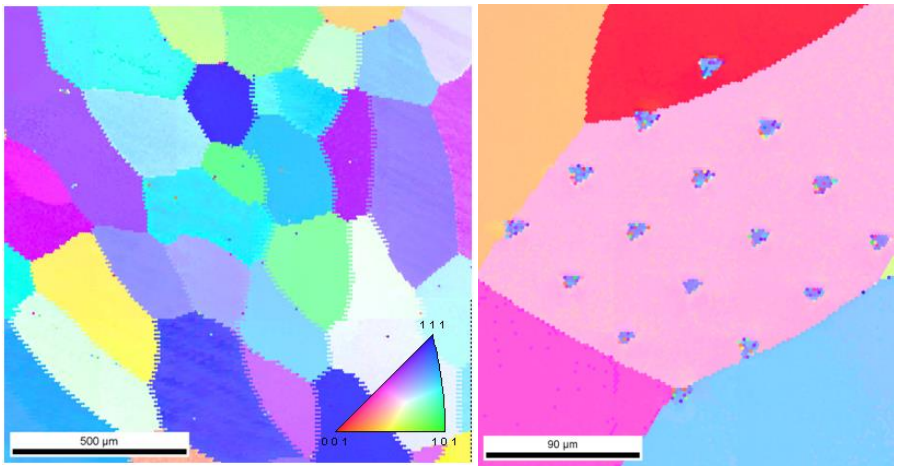

Figure 1 *- Inverse Pole Figure EBSD maps of surface normal direction of grain structure for a typical indentation site in pure W (unimplanted).*

The helium implantation was carried out at the National Ion Beam Centre, University of Surrey, using a 2MV tandem accelerator (HVEE, Netherlands) The implantation was carried out at ~300°C using a range of energies: 0.05, 0.1, 0.2, 0.3, 0.4, 0.6, 0.8, 1.0, 1.2, 1.4, 1.6 & 1.8 MeV, with fluences of $3.6x10^{15}$, $1.5x10^{15}$, $5x10^{15}$, $1.0x10^{15}$, $5.0x10^{15}$, $5.0x10^{15}$, $5.0x10^{15}$, $5.0x10^{15}$, $5.0x10^{15}$, $5.0x10^{15}$, $5.5x10^{15}$ and $6.0x10^{15}$ ions/cm^2 respectively, to produce a relatively flat implantation profile, as shown in figure 2. Profiles were calculated using SRIM (Stopping Range of Ions in Matter), assuming a displacement energy of 68eV [16]. Fluences were chosen to produce an implanted concentration of close to 3000appm over the implantation depth range.

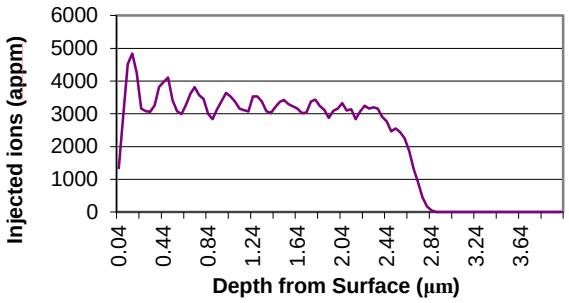

Figure 2 *– SRIM calculated He profile in pure W for ~3000appm implantation.*

RESULTS & DISCUSSION

Unimplanted alloys

Figure 3 shows indentation hardness and modulus values as a function of alloy composition. Values are shown as an average of a minimum of 16 indents over the 200-300nm indenter depth range. This range was chosen for later comparison with data of implanted materials from self-ion implantation experiments, in which, below 75nm indentation depth, the data are dominated by tip shape effects and initial pop-in and above 400nm the data become dominated by the unimplanted

'substrate' [12]. The compositions tested in both species fall well within their solubility limits in tungsten [17-18].

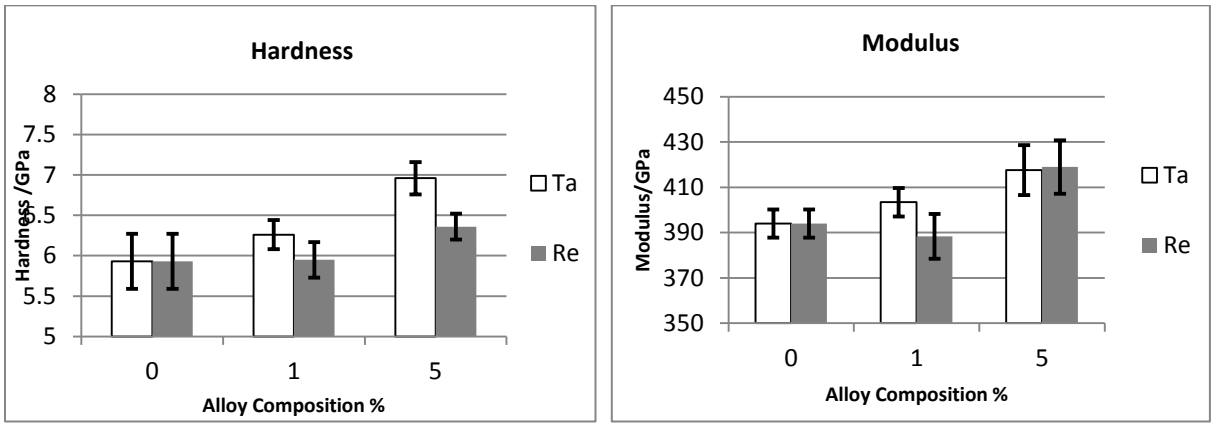

Figure 3 *- Indentation hardness & modulus for all W-Re & W-Ta compositions (error bars 1 standard deviation).*

The numerical hardness values alongside with the % change from pure W can be seen in table 1. Although there is slight trend of increasing hardness with composition in both W-Ta and W-Re alloys the only sample which shows a substantial increase is W-5%Ta, where the increase falls well outside of any potential error. The results also show a small increase in modulus at both 5% compositions, although this increase is negligible.

Table 1 – *Change in hardness and modulus of unimplanted samples as with composition.*

Composition	Hardness /GPa	ΔHardness /GPa	% Change	Modulus /GPa	ΔModulus /GPa	% Change
Pure	5.93±0.34	-	-	394.0±6.27	-	-
1Ta	6.26±0.18	0.33±0.52	6	403.4±6.28	9.40±12.55	2
5Ta	6.96±0.20	1.03±0.54	17	417.6±11.0	23.6±17.27	6
1Re	5.95±0.22	0.02±0.56	0	388.3±9.91	-5.70±16.18	-1
5Re	6.36±0.16	0.43±0.50	7	419.0±11.8	25.0±18.07	6

He Implanted

Figure 4 shows the modulus and hardness in the helium implanted materials compared with their unimplanted state, with the numerical values shown in table 2. It can be seen that the Ta alloys harden after implantation slightly more in absolute terms than the Re alloys. With the W-Re alloys the increase in hardness due to implantation increases with solute content , but this trend is reversed in the W-Ta alloys, with the W-5%Ta concentration sample hardening slightly less than the W-1%Ta alloy. The overall hardening effect is greater in the W-Ta alloys than the W-Re compositions. The proportional increase in hardening can be seen in table 2, with a reduction in the alloyed samples, especially in the W-5%Ta. The proportional change in the W-Re alloys remains approximately the same.

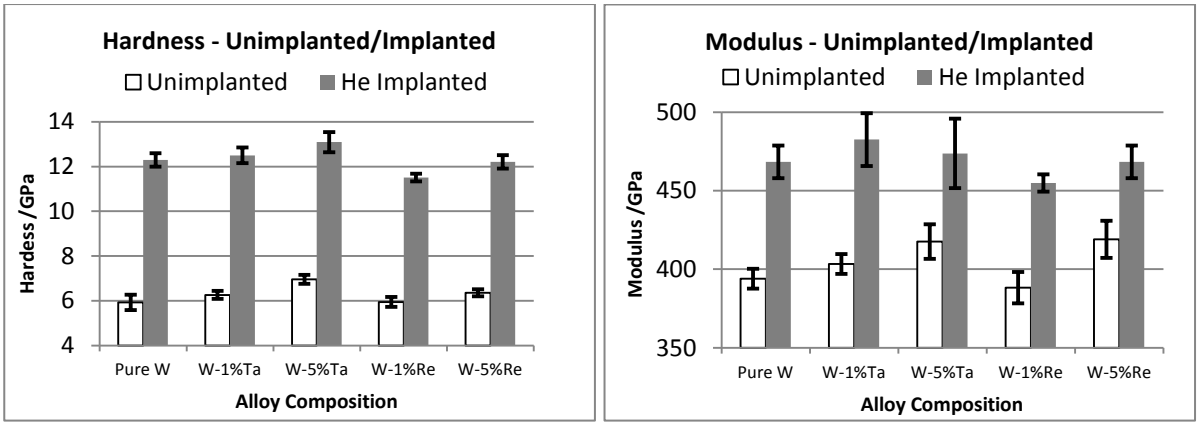

Figure 4 *- Indentation Hardness & Modulus for all W-Re & W-Ta compositions implanted with 3000appm He (error bars 1 standard deviation).*

Figure 4 and Table 2 also show that there is an appreciable increase in modulus of all the samples after implantation. As with the increase in hardness, the increases in modulus are marginally higher in the W-Ta alloys than the W-Re alloys, with a reduced increase in the W-5% alloy concentration samples in both the W-Re and W-Ta compositions.

Table 2 – *Change in hardness and modulus from unimplanted to 3000appm He implanted*

Composition	Hardness /GPa	% Increase	Modulus /GPa	% Increase
Pure	6.36±0.64	107	74.4±16.67	19
1Ta	6.24±0.53	100	79.1±23.18	20
5Ta	6.13±0.65	88	56.1±33.10	13
1Re	5.56±0.39	93	66.5±15.41	17
5Re	5.85±0.46	92	49.4±22.20	12

Initial transmission electron microscopy (TEM) of the pure W sample implanted to 3000appm He revealed that no visible He bubbles had formed (figure 5). This indicates that the He in the sample exists as small He-vacancy clusters below the resolution limit of the TEM. Such small He-vacancy clusters may be the source of the observed increased hardening via He-vacancy cluster pinning of mobile dislocations.

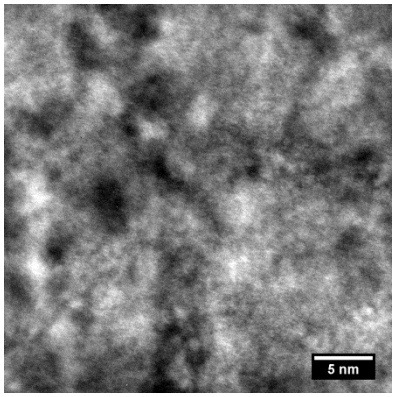

Figure 5 *– TEM micrograph of the 3000appm He implanted pure W. The image was recorded at ~1µm underfocus. No Fresnel contrast was observed in a through-focus series indicating no He bubbles are present.*

Conclusions

The effects of alloy composition on hardness and modulus in dilute W-Re and W-Ta model systems likely to be of interest in fusion are relatively small. However helium implantation can have an extremely significant effect on hardness of tungsten alloys, particularly at high He concentrations. These effects are substantially greater than those of self-ion implantation (cascade damage) alone [12]. Helium-irradiation hardening and associated brittleness could have significant repercussions on the use of such alloys in structural alloy components

Acknowledgements

This work was funded by the EPSRC through the Programme Grant "Materials for Fusion and Fission Power" (EP/H018921/1). DEJA thanks the support of CCFE via a Junior Research Fellowship at St Edmund Hall, Oxford. CEB also thanks the Worshipful Company of Armours and Braziers for their support. We gratefully acknowledge the assistance of researchers and staff at the National Ion Beam Centre, University of Surrey, UK and the Department of Materials Science & Metallurgy at the University of Cambridge, UK.

References

1. Baluc. N., et al, Nuclear Fusion, **47**, ppS696-S717 (2007)
2. Yoshida. N., Journal of Nuclear Materials, **266-269**, pp197-206, (1999)
3. Baldwin. M. & Doerner. J, Nuclear Fusion, **48**, pp1-5, (2008)
4. Xu Q., et al., Materials Transactions, **46**, 6, pp1255-1260, (2005)
5. Norajitra. P., et al., Journal of Nuclear Materials, **367-370**, B, pp1416-1421, (2007)
6. Causey. R. & Venhaus, T., Physic Scripta, **T94**, pp9-15, (2001)
7. Baluc. N., et al., Nuclear Fusion, **47**, ppS696-S717, (2007)
8. Rieth. M. & Hoffmann. A., International Journal of Refractory Metals and Hard Materials, **28**, pp679-686, (2010)
9. Gilbert. M., & Sublet. J-Ch., Nuclear Fusion, **51**, 4, (2011)
10. Reith. M., et al, Journal of Nuclear Materials, **432**, 1-3, pp482-500, (2013)
11. Lewis. M., et al., Nuclear Instruments and Methods, **167**, pp233-247, (1979)
12. Armstrong. D. E. J., et al., Journal of Nuclear Materials, **432**, 1-3, pp428-436, (2013)
13. Hardie. C. D., & Roberts. S. G., Journal of Nuclear Materials, **433**, 1-3, pp174-179, (2013)
14. Zenobia. S. J., et al., Journal of Nuclear Materials, **425**, 1-3, pp83-92, (2012)
15. Oliver. W. C. & Pharr. G. M., Journal of Materials Research, **7**, 1564-1583, (1992)
16. International A. ASTM E521 – 96 (2009), Standard Practice for Neutron Radiation Damage Simulation by Charged-Particle Irradiation, 2009, ASTM International, West Conshohocken, PA
17. Ayres. R., et al., Journal of Applied Physics, **46**, 4, pp1526-1530, (1975)
18. National Physical Laboratories, MTDATA Calculated Phase Diagram, http://resource.npl.co.uk/mtdata/phdiagrams/taw.htm